



Response Mechanism of Mechanical Behavior with Mg Plate Microstructure Evolution During Al/Mg/Al Composite Plate Rolled by hard Plate

Rong He Gao¹ · Feng Li^{1,2,3} · Wen Tao Niu¹ · Peng Da Huo¹

Received: 1 September 2022 / Accepted: 9 November 2022 / Published online: 14 December 2022

© The Author(s) under exclusive licence to The Korean Institute of Metals and Materials 2022, corrected publication 2023

Abstract

The long manufacturing process, difficult coordinated regulation of structural properties and interface bonding ability are some of the difficulties that restrict the rapid development of lightweight composite plate forming and manufacturing for a long time. In order to solve the above problems, this paper proposes adding hard plate to roll Al/Mg/Al composite plates. The thickness of Mg/Al is 10:1, and the hard-plate rolling process experiments were carried out by designing five groups of different temperatures. The influence of magnesium plate microstructure evolution on the interface bonding ability and mechanical behavior of composite plates is mainly studied. Under the same conditions, the matrix microstructure changes greatly from 200 to 350 °C. At 350 °C, the microstructure of Mg plate in ND is uniform without shear bands and twins. Its recrystallization ratio is 31.77%, which played a role in weakening the texture and reducing its anisotropy. Interestingly, in the process of three-point bending, the non-basal plane slip and the basal plane slip start simultaneously, the maximum bending strength of the composite plate reaches 504 MPa, and the interface was well bonded without obvious bending fatigue phenomenon. The tear test showed that the tear load reaches 0.42 kN, and the elastic elongation stage of Al is longer than the tear propagation stage, and the interface bonding was uniform. The hard plate rolling process provides scientific guidance for the forming and preparation of composite plates.

Keywords Hard-plate hot rolling · Al/Mg/Al composite plate · Microstructure · Mechanical properties · Interface bonding strength

1 Introduction

Because it can realize the complementary advantages of each single board component and achieve the gain effect, the consumption of lightweight high-performance composite boards has increased sharply in recent years and has been widely used in weapons and equipment, rail transit, energy and chemical industries, and other fields [1–3]. Taking Al/Mg/Al composite plate as an example, this “sandwich” structure can have the corrosion resistance of Al alloy [4] and at the same time have the characteristics of light specific gravity and high specific strength of Mg alloy [5–7]. However, how to prepare high-performance composite boards has always been a troublesome problem. Many existing processes can be used to prepare composite boards, but the performance of composite boards, especially the interface bonding ability, is difficult to guarantee.

Tang et al. [8] prepared Al/Mg/Al composite plates by porthole die co-extrusion (PCE). The results showed that

✉ Feng Li
fli@hrbust.edu.cn

Wen Tao Niu
tao364904899@163.com

¹ School of Materials Science and Chemical Engineering, Harbin University of Science and Technology, Harbin 150040, People’s Republic of China

² Key Laboratory of Advanced Manufacturing and Intelligent Technology, Ministry of Education, Harbin University of Science and Technology, Harbin 150080, People’s Republic of China

³ Heilongjiang Provincial Key Laboratory of Light Metal Materials Modification & Green Forming Technology, Harbin 150040, People’s Republic of China

there was a two-layer diffusion layer at the Al/Mg interface, and its width was changed significantly with the change of temperature and reduction ratio. But in the aluminum layer and magnesium layer appeared coarse grains and accompanied by strong texture. Chen et al. [9] also used the (PCE) method to prepare Al/Mg/Al composite plates. The results showed that the composite plates prepared by the PCE method had no obvious defects at the Al/Mg interface and played a certain role in weakening the texture. The hardness of the interface was lower than that of the matrix.

Bi et al [10] proposed a new method of 'full coverage + stir friction welding + cumulative roll welding' to prepare Al/Mg/Al composite plate. The experimental results showed that under the condition of 400 °C and single pass processing, there was no obvious defect at the interface junction and the edge damage was the smallest. After subsequent heat treatment, the diffusion layer of the composite plate was obviously thickened and its performance was improved to a certain extent. Yang et al. [11] found that the Al/Mg/Al composite plate prepared by vertical explosive welding (EXW) would produce corrugated bonding morphology at the interface junction, forming Al/Mg mechanical interlocking to improve the bonding strength of Al/Mg plate. But there were dangerous, not environmental protection, defects and other deficiencies.

In order to study the effect of rolling process on the microstructure, interface bonding and mechanical properties of Al/Mg/Al composite plate, Yu et al. [12] prepared Al/Mg/Al composite plate by hot rolling. Through the research, it was found that the process can promote the diffusion of elements at the interface to improve the compactness of the microstructure, and the fracture mode of the composite plate was changed from intergranular fracture to ductile fracture. In order to better prepare high-performance Mg/Al composite plates, Sun et al. [13] studied the effects of rolling process parameters on the microstructure and mechanical properties of Al/Mg/Al composite plates. Studies had shown that the Al plate exhibits a non-uniform hardness distribution from the surface layer to the interface junction showing a gradual decline. The proportion of recrystallized grains at the center of the magnesium layer increased with the increase of reduction and temperature, and incomplete crystallization occurs at the interface junction.

By comparison, it can be seen that the rolling method is still the main method for forming and manufacturing high-performance lightweight composite sheets and is widely used [14–16]. The existing research results showed that adding hard plates could convert part of the roll shear stress into compressive stress [17]. However, due to the change in process conditions, it was more difficult to control the microstructure and uniformity, and it had an important impact on the interface bonding ability of composite plates. This paper takes this as the center for research.

2 Research Proposal

2.1 Process Principle

The existing research results show that the addition of hard plate can achieve a large reduction in deformation in a single pass for the rolling of Al/Mg/Al composite plates. Hard-plate rolling is an effective way to realize the preparation of high-performance composite plates [18]. In the rolling process, the existence of the hard plate increased the compressive stress in the ND direction of the indirect contact between the composite plate and the roll, formed a metal flow velocity difference between Mg and Al, and then formed a mechanically interlocked interface bonding morphology, which significantly improved the performance. The preparation of light sheet by large reduction could also eliminate the shear band, reduce the shear deformation in the subsequent processing of composite plate, and realize the homogenization of structure. The process principle is shown in Fig. 1.

In order to promote the more effective diffusion of Mg/Al atoms during the rolling process, the surface of AZ31 B magnesium alloy and AA1060 A aluminum alloy slab was polished by sandpaper before rolling, and it was placed in acetone solution for degreasing. The surface of the plate was washed with alcohol and dried naturally. To ensure that the composite slab is not separated during the rolling process, it is fixed with a 0.3 mm diameter wire. In order to prevent the adhesion between the liner and the composite plate during the rolling process due to the effect of compressive stress, a layer of high temperature isolating agent (boron nitride) was uniformly sprayed between the two, and stacked in the order shown in Fig. 1. The composite specimens were heat treated, holding time was 20 min, rolling temperature k was 200 °C, 250 °C, 300 °C, 350 °C, 400 °C. The experimental equipment is a two-roll mill with a speed of 6 rad/s and a single pass reduction of 65%. After preheating, the fixed end of the plate was sent to the rolling mill and air-cooled to room temperature.

The research materials were AZ31B plate with thickness $t_1 = 2$ mm and AA1060 plate with thickness $t_2 = 0.2$ mm. The chemical composition is shown in Table 1. The outermost side was S304 stainless steel plate with hard plate $t_3 = 1$ mm.

2.2 Characterization of Mechanical Properties

A Scanning electron microscope (SEM) was used to observe the interface connection morphology of the hard plate rolling composite plate. A three-point bending specimen with a length of 80 mm and a width of 5 mm was cut

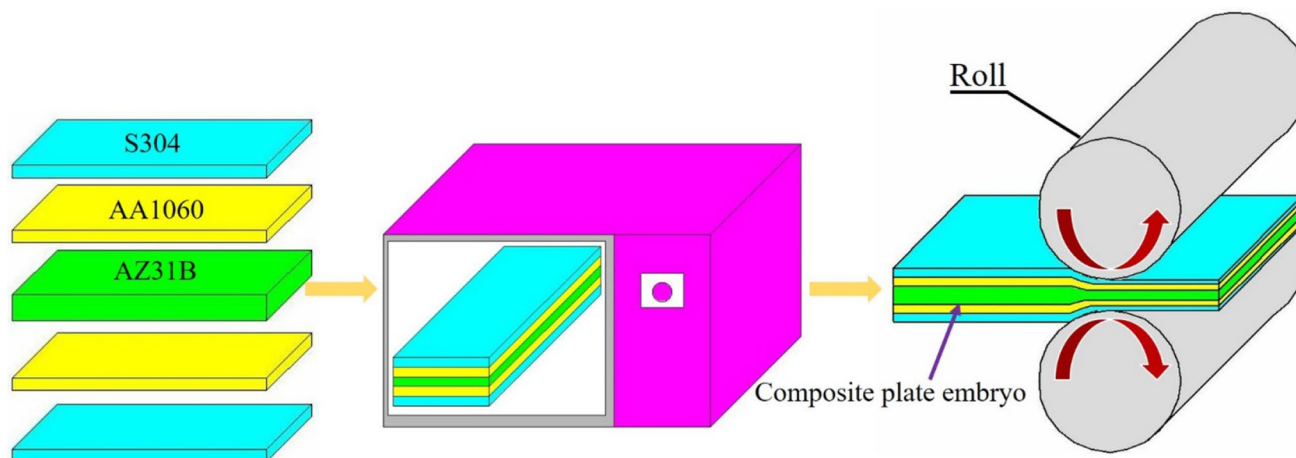


Fig. 1 Process principle of hard-plate rolling Composite Plate

Table 1 Composition table of AZ31B Mg alloy and AA1060 Al alloy

| Materials | Mg | Al | Mn | Cu | Fe | Zn | Ca |
|-----------|-------|------|-------|------|-------|------|------|
| AZ31B | 95.45 | 3.9 | 0.334 | 0.05 | 0.005 | 0.81 | 0.04 |
| AA1060 | 0.03 | 99.6 | 0.03 | 0.05 | 0.35 | 0.05 | – |

at the center of the composite plate by wire cutting, and the three-point bending specimen was tested many times by a universal material testing machine to obtain the average value. A 100 mm long and 40 mm wide specimen was cut in the middle of the composite plate for the tear resistance test, and the average value of multiple groups of tests was taken to ensure its accuracy. A sample with a length \times width of 6 mm \times 4 mm was cut by wire cutting technology, and 400 #, 800 #, 1500 #, 3000 #, 5000 # and 7000 # sandpaper were used for grinding, and then mechanical polishing was carried out to completely eliminate the influence of scratches on the hardness of the sample surface. The hardness of different parts of the composite plate was tested by Vickers hardness tester under the condition of 25 g holding load, 10s holding time and 20 °C holding temperature.

2.3 Microstructure Characterization

Observe the metallographic structure with an electron microscope (OM), and cut the EBSD sample in the ND direction on the magnesium side by wire cutting. The size of this specimen is 6 mm long and 4 mm wide. Abrasive papers of 400, 800, 1500, 3000, 5000, and 7000 grits, respectively, were used for grinding, followed by mechanical polishing and electrolytic polishing. The electrolytic polishing liquid was a mixture of phosphoric acid and alcohol, and the polishing time was set according to the difference in sample position. After electrolysis, use alcohol to quickly clean the surface

of the sample. Finally, we tested using a Quanta 200 F field emission scanning electron microscope. The Channel 5 software was used to denoise the original data standard and analyze EBSD data.

3 Results

3.1 Scanning of Interfaces

The interface bonding morphology was an important index to reflect the performance of the composite plate, so the scanning electron microscope (SEM) was used to analyze the interface morphology of the composite plate under different conditions, as shown in Fig. 2. When the temperature was k_1 , that is 200 °C, the interface bonding morphology and diffusion layer thickness were shown in Fig. 2a. It could be found that the Al/Mg bonding interface was basically not welded, resulting in a large gap, and there were only small connecting parts. At low temperatures, it was almost impossible to produce the mutual flow of Mg/Al elements to form the bonding morphology of mutual separation. At k_2 , that is 250 °C the metallurgical bonding of the Mg/Al interface was realized, as shown in Fig. 2b, but the forming temperature was low, the metal flow rate was slow, and the Mg and Al matrix at the interface were broken under the action of large reduction, and the broken layer thickness reaches 15 μ m while the interface only accounts for about one third. Figure 2c shows the interface bonding morphology and

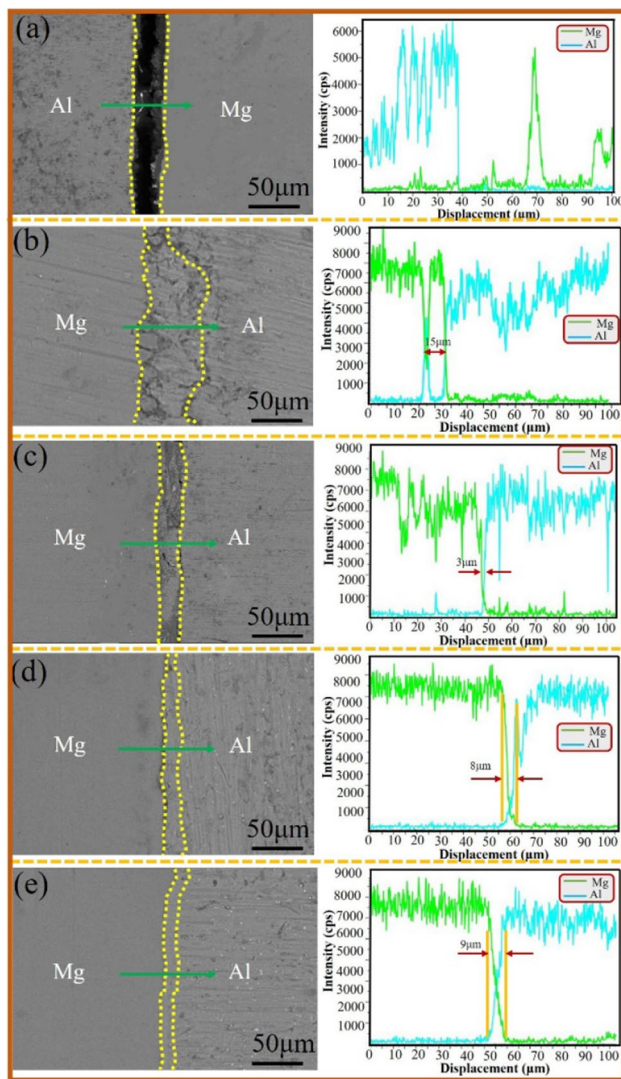


Fig. 2 Al/Mg/Al interface morphology and line scan: **a** k_1 ; **b** k_2 ; **c** k_3 ; **d** k_4 ; **e** k_5

diffusion layer thickness under the condition of 300 °C, that is k_3 . As shown by the figure, compared with k_2 , the brokenness of the matrix was greatly reduced, but the broken Al matrix still exists in the rolled state, and the thickness of the interface diffusion layer was only 3 μm . Figure 2d shows the interface bonding morphology at 350 °C. From Fig. 2d, it could be found that there were no defects such as pores and impurities at the interface bonding and the bonding was good. Under the condition of thermal deformation, the metal flow velocity at the interface increases, and the flow velocity difference occurs at the interface of different substrates, so that the joints show local protrusions and depressions so as to achieve the effect of mechanical interlocking. The interface bonding morphology at k_5 is shown in the Fig. 2e, there are still local bulges and depressions, and the thickness of the interface diffusion layer is slightly greater than k_4 .

3.2 Tear Properties

The tear test is one of the main methods to test the interface bonding ability of composite plates, and it is the most clearly demonstrated interface bonding uniformity and strength of composite panels in various mechanical tests. Figure 3 shows the test curves for the tearing properties of Al/Mg/Al composite plates under different conditions. One part of the Al/Mg bonding layer on both sides of the composite plate was torn off, and one side was fixed with rivets, as shown in Fig. 3a, and the tearing performance was tested. Figure 3e shows the tearing curve at k_4 . It could be observed that compared with other conditions, the tearing curve tended to be stable as a whole, without obvious breakpoints and sharp increases, and the maximum load reaches 0.42 kN, and the minimum was 0.33 kN indicates that the bonding of Mg/Al interface was relatively uniform. In the partial enlarged view, there was a period of elastic deformation of Al before reaching the initial tearing point (purple ellipse) with a length of (a) As the tensile load increased, it gradually reached the initial tearing point and the length of the tearing process was the tear expansion stage of (b) When the load reaches the initial tearing point, the separation between Al and Mg begins, and in the tearing process, the separation along with the surrounding Al plate also occurs. That was the tear propagation stage. It could be found from Fig. 3e that the length a of the elastic elongation stage of Al is greater than the length b of the tear expansion process, and the load begins to gradually decrease after reaching the initial tear point, under the action of which the surrounding Al plate is stressed and gradually separated from the Mg plate, but stops immediately after the expansion length reaches b. It could be seen from 3.1 that the interface was only partially welded at k_1 , so the tearing curve showed a platform area composed of a large number of straight lines and the load was very small. At k_2 , a large number of broken areas appear at the interface, which greatly reduces the tearing load compared with k_4 . From Fig. 3c, it could be found that the curve fluctuation was very large and the interface bonding was rather uneven. The tearing curve at k_3 is shown in Fig. 3d. From the above analysis, it could be seen that the layer thickness was only 3 mm, so the tearing load was relatively low, and the degree of uniformity of interface bonding was significantly improved compared with that of k_2 . Figure 3f shows the tearing curve at k_5 . Although the tearing load was slightly increased, the interface bonding was not uniform.

3.3 Bending Performance

In order to explore the effect of interfacial bonding ability on the properties of the composite plate, the three-point bending performance test of the Al/Mg/Al composite plate and the SEM of the specimen after the test are shown in Fig. 4.

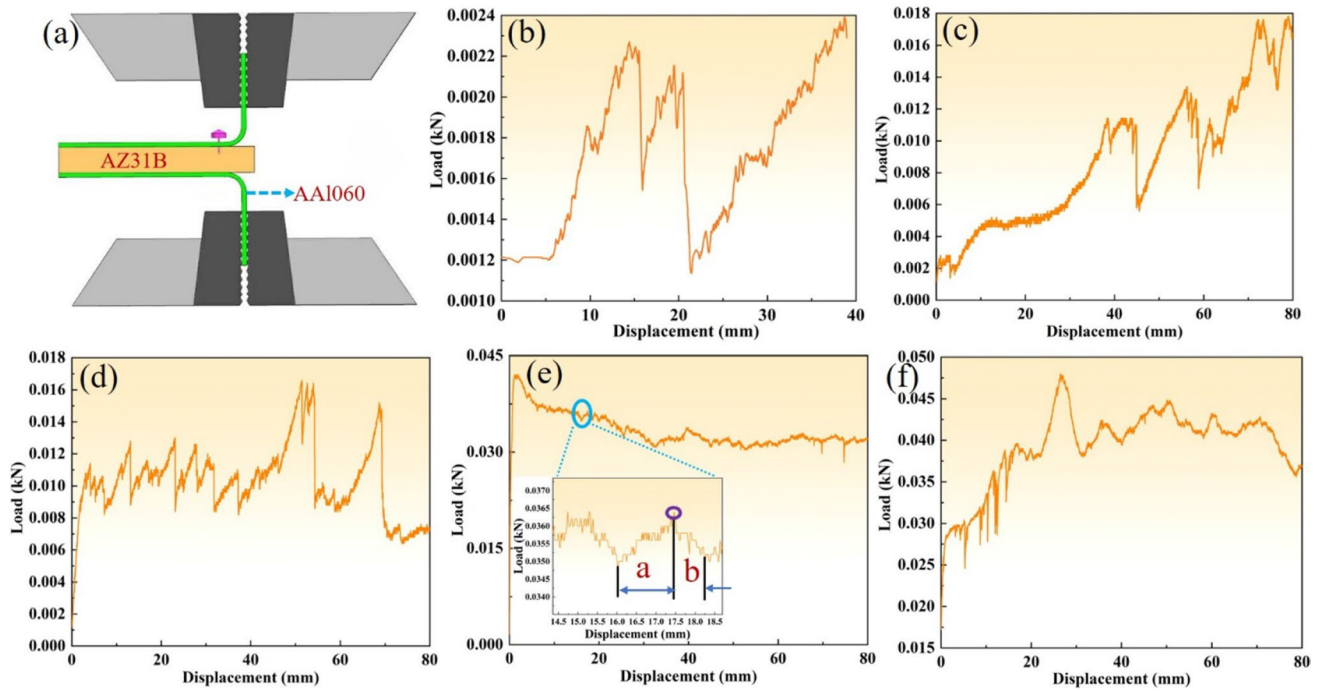


Fig. 3 Al/Mg/Al interface morphology and line scan **a** Schematic Diagram; **b** k₁; **c** k₂; **d** k₃; **e** k₄; **f** k₅

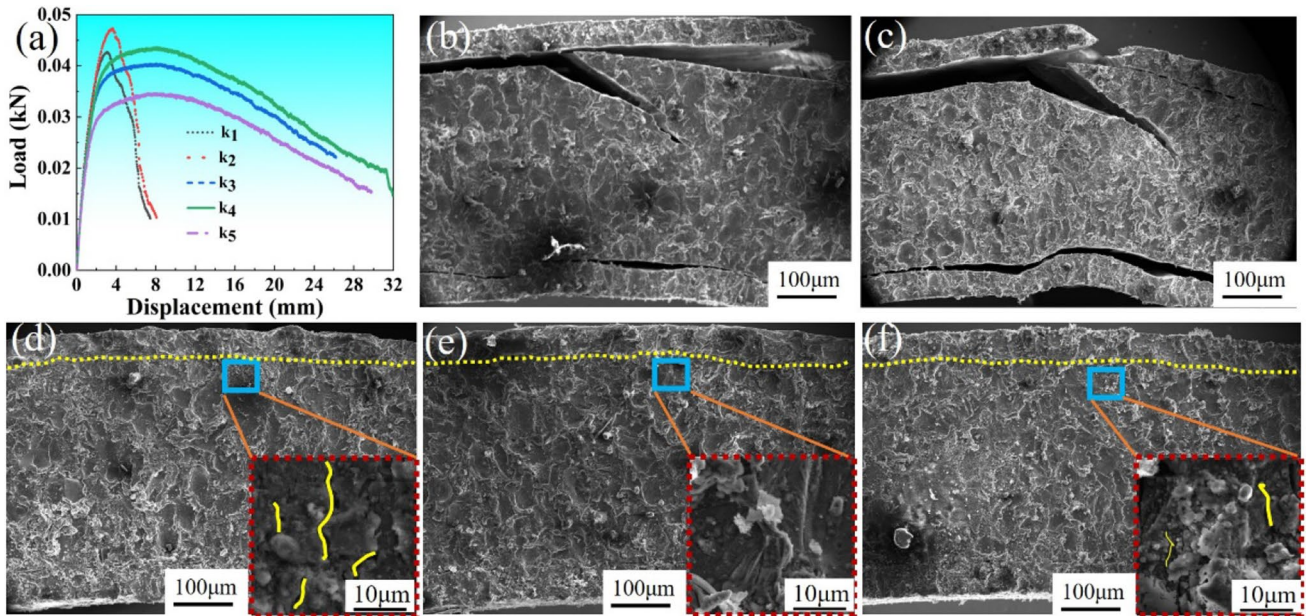


Fig. 4 Three-point bending performance test of Al/Mg/Al composite plate **a** Three-point bending performance curve; **b–f** Sample scanning after bending

Figure 4a is the three-point bending test curve of the Al/Mg/Al composite plate under different conditions. Due to the small size of the sample in the experiment, the cross-section of the sample gradually changed from a rectangle to a fan shape during the bending process, and the thickness was

reduced, resulting in a gradual decrease in the load. It could be seen from Fig. 4a that the curve presents three deformation stages of elasticity, yield, and instability. The buckling phase was very short at k₁ and k₂, and fracture occurs when the plastic deformation during bending is very small. At k₄,

the buckling stage dominates and reaches 28.4 mm, and it reaches its maximum load of 0.0349kN in the yield stage. The maximum flexural strength formula [19] is shown in (1)

$$\sigma_{bb} = 3pl/2bh^2 \tag{1}$$

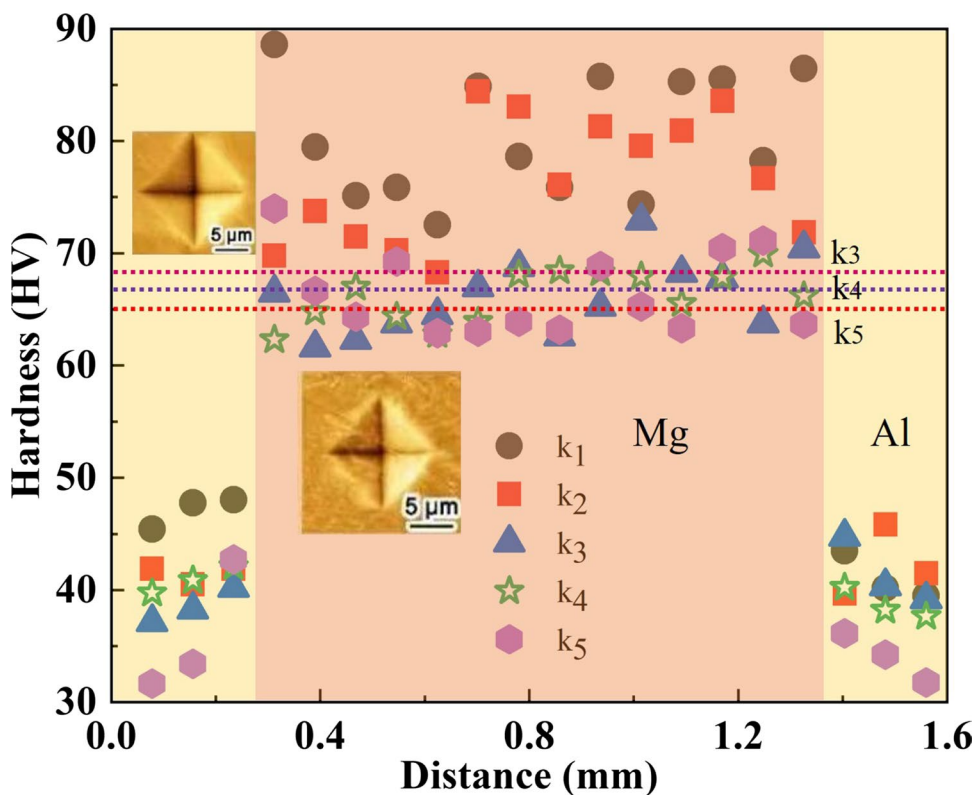
σ_{bb} is the tensile strength; P is the ultimate bending load; l is the span; b is the sample width; h is the sample thickness, and l/bh^2 is defined as the size factor. From 2.3, it could be known that $b = 5 \text{ mm}$, $l = 48 \text{ mm}$, $h = 1 \text{ mm}$. According to formula (1), the maximum flexural strength is 504 MPa. At k_3 , the buckling stage was 22.3 mm and the load was 0.038kN, both smaller than k_4 , and its plastic deformation capacity and maximum flexural strength were not as good as k_4 . The plastic deformation ability of k_5 was almost the same as that of k_4 , but the bending strength was far less than that of k_4 . Figure 4e was the SEM scanning image of the bending specimen at k_4 , from which it could be found that there was no obvious phenomenon of micro-cracks due to fatigue damage at the outer Mg matrix of the bending, and the Mg/Al interface was still tightly bonded, as could be seen from the enlarged image no obvious micro-cracks were generated at the interface joint. When the composite sheet was subjected to external stress during bending, the interface between the different matrices in the “sandwich” structure provided stress transformation, with weak interfaces far from the indenter being compressive and strong interfaces

closed to the indenter being subjected to tensile stress, a stress state in which the tensile and compressive stresses of pulling up and pressing down were transformed into each other in the composite board. The failure of composite panels usually originates from weak interfaces between different matrices. Due to the obvious destruction of weak interfaces by compressive stress, the bottom interface far away from the indenter is crucial to the bending properties of the laminates, resulting in improved bending properties of the composites. Compared with k_4 , k_3 and k_5 , there were small microcracks in the Mg matrix at the interface joint after bending, as shown in Fig. 4d, f, but the microcrack of k_5 was obviously smaller than that of k_3 .

3.4 Microhardness

Hardness testing is one of the most practical means of measuring sheet properties. When measuring different metals, Vickers hardness is the most accurate compared to Brinell and Rockwell indices. The hardness is related to the resistance of the material to plastic deformation. Mg alloys have a close-packed hexagonal structure, while Al alloys are face-centered cubic, so the hardness of Mg is much greater than that of Al [20]. Figure 5 shows the comparison of the Vickers microhardness in the thickness direction of the Al/Mg/Al composite plate under different conditions. It was measured under the conditions of 25 g holding pressure and time, 10 s,

Fig. 5 Hardness and microhardness of Al/Mg/Al composite plate under different conditions



and temperature of 20 °C. As shown by the figures, the hardness of the Mg matrix at k_1 and k_2 fluctuates greatly compared with other conditions, and the average hardness was high, which was due to the localized work hardening during the rolling process under the low temperature forming condition, which made the hardness very uneven. As it was k_3 , the average hardness of the Mg matrix was 68.31 HV. As shown by the yellow straight line in the figure, it could be found that the hardness fluctuates in waves near the average hardness. The average hardness at k_4 was 66.17 HV (black straight line). The figure shows that the hardness values fluctuate in a small range around the average hardness, and the Mg matrix structure is relatively uniform compared to other conditions. The red line in the figure was the average hardness of 64.58 HV at k_5 . At high temperatures, the softening hardness of the Mg matrix decreased and the uniformity was slightly inferior to that of k_4 . The figure showed that the hardness of the Mg side was relatively uniform and had been fluctuating around the average hardness, while the hardness of the Al side was a phenomenon where the hardness increased significantly near the interface joint. Since the rolling temperature was lower than the recrystallization temperature of aluminum, the Al matrix was partially work hardened during the rolling process [21], forming a brittle and hard phase at the interface, which increases the hardness of the Al side. Since the volume fraction of the Mg matrix is as high as 83.3%, the hardness of Mg at the interfacial junction was not significantly improved.

4 Discussion

It can be seen from the above analysis that, under k_4 condition, the overall performance of the Al/Mg/Al composite plate is the best under different conditions. Because the Mg/Al ratio used in this paper is 10:1, the influence of Mg plate structure on the overall performance of composite plate is much greater than that of Al plate. Therefore, the microstructure of magnesium matrix under k_4 condition was investigated by metallographic and EBSD analysis.

4.1 Microstructure

Because the stress state and deformation behavior of each layer of the composite plate were changed after the rolling was added, the evolution of the microstructure was very different from traditional rolling [22]. Figure 6 shows the ND-direction microstructure of the magnesium sheet in the hard-plate rolled composite plate under different conditions.

In the traditional rolling, the sheet structure exhibits anisotropy due to shear deformation. Hard plate rolling can partially convert the shear force into pressure, so under the action of the rolling, the adverse effects caused by the anisotropy of the structure could be appropriately weakened. Figure 6a shows the metallographic structure at k_1 . It could be seen from the figure that there were shear bands composed of broken grains and a small amount of dynamic recrystallization, as well as a large number of sheet twins (red

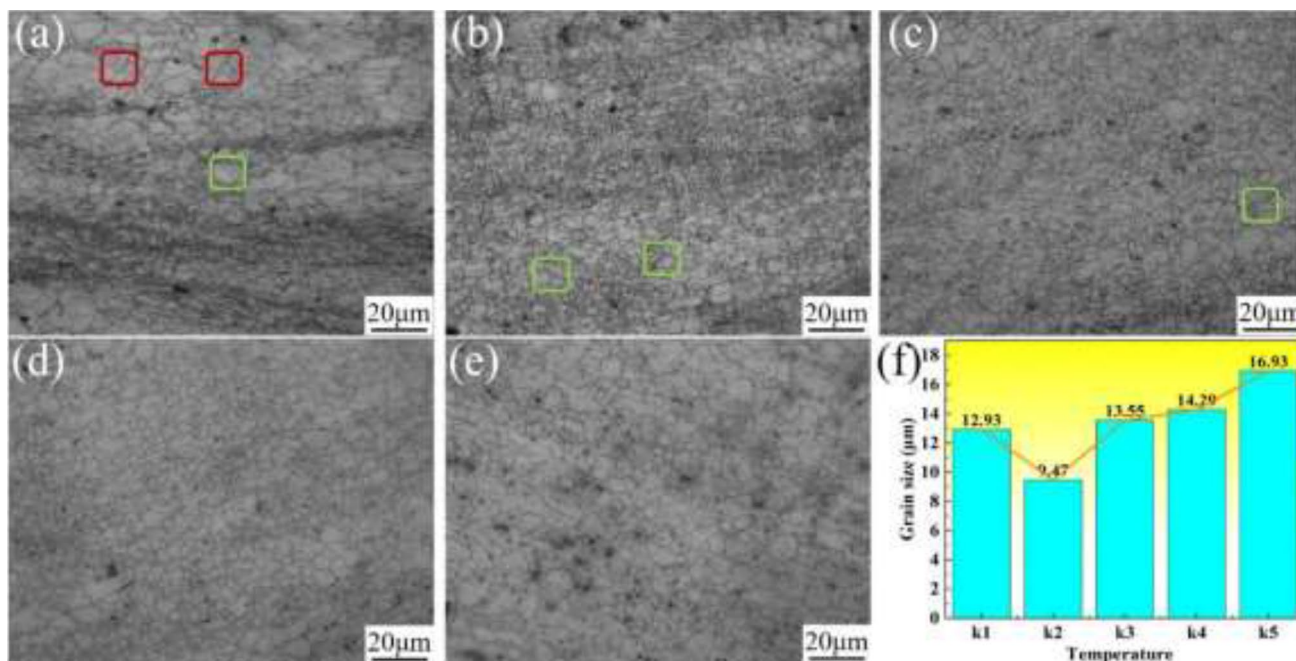


Fig. 6 Microstructure of hard-plate rolled magnesium sheet under different conditions **a** k_1 ; **b** k_2 ; **c** k_3 **d** k_4 ; **e** k_5 ; **f** Grain size

box) and a small number of flat twins (blue box), with an average grain size of 12.93 μm . During dynamic recrystallization, the existence of sheet twins inhibits the energy for their nucleation process [23]. At the same time, the existence of twins would promote crack nucleation. When twins intersect with grain boundaries, the stress near the interface may be highly concentrated, which may induce cracks. The structure of the Mg matrix at k_2 was shown in Fig. 6b. Due to the increase in deformation temperature, the twins were greatly reduced, but there were still shear bands. In the subsequent shear deformation, cracks would be generated at the shear bands, which was not conducive to the subsequent processing of the composite plate, with an average grain size of 9.47 μm . When the temperature was k_3 , as shown in Fig. 6c, the shear band disappeared and a large number of equiaxed grains appeared, but there were some coarse grains with uneven grain morphology and an average grain size of 13.55 μm . At k_4 , the microstructure was dominated by equiaxed grains without coarse grains, and the homogenization was greatly improved. Compared with k_3 , the average grain size did not change significantly. When the rolling temperature was further increased, the uniformity of the structure changed significantly, but the grains grew significantly, and the grain size was 16.93 μm .

4.2 Magnesium Plate Inverse Pole Figure (IPF)

It can be seen from the above analysis that the ND of the magnesium sheet in the Al/Mg/Al composite sheet presents the phenomenon of uniformity of the structure. The preferred orientation of grains in the organization is called texture, and texture can have a great impact on the properties of

the material, so the material is subjected to EBSD analysis. The IPF map is taken to analyze the texture characteristics and grain orientation difference of the material. The IPF color image, pole figure and orientation distribution of the magnesium plate are shown in Fig. 7. It can be found from Fig. 7a that the microstructure of the magnesium plate is dominated by fine grains, and some dark-colored coarse deformed grains occasionally appear. In the deformed grains, it can be observed that a large number of sub-grain boundaries were continuously accumulated in the grains due to the obstacles encountered in the movement of dislocations. This large number of sub-grain boundaries provided energy for the nucleation of subsequent recrystallization. The main orientation of deformed grains was (0001) basal plane orientation, and there is a large amount of recrystallization in the structure. The grains are relatively uniform, with a high degree of refinement, and the grain orientation is relatively free. From the polar diagram in Fig. 7b, it can be seen that the region with the highest density was mainly distributed in the ND, that is the grain orientation \perp RD. Due to the application of the hard plate, the shear-force of the roll is partially converted into the compressive stress in the ND. Under the joint action of the shear force in the RD, the grains are twisted and then show the basal texture deflected in the ND, and the maximum polar density point of the basal plane is 13.44. It can be seen from the grain boundary orientation in Fig. 7b that the grain boundary orientation is mainly concentrated in the sub-grain boundary ($< 2^\circ$) formed by dislocation packing, accounting for about 29.9%, and reaches a peak at the orientation of 1.5° , indicating that the Error density is high. The low-angle grain boundaries (LAGBs, $< 15^\circ$) caused by the movement and rearrangement of accumulated

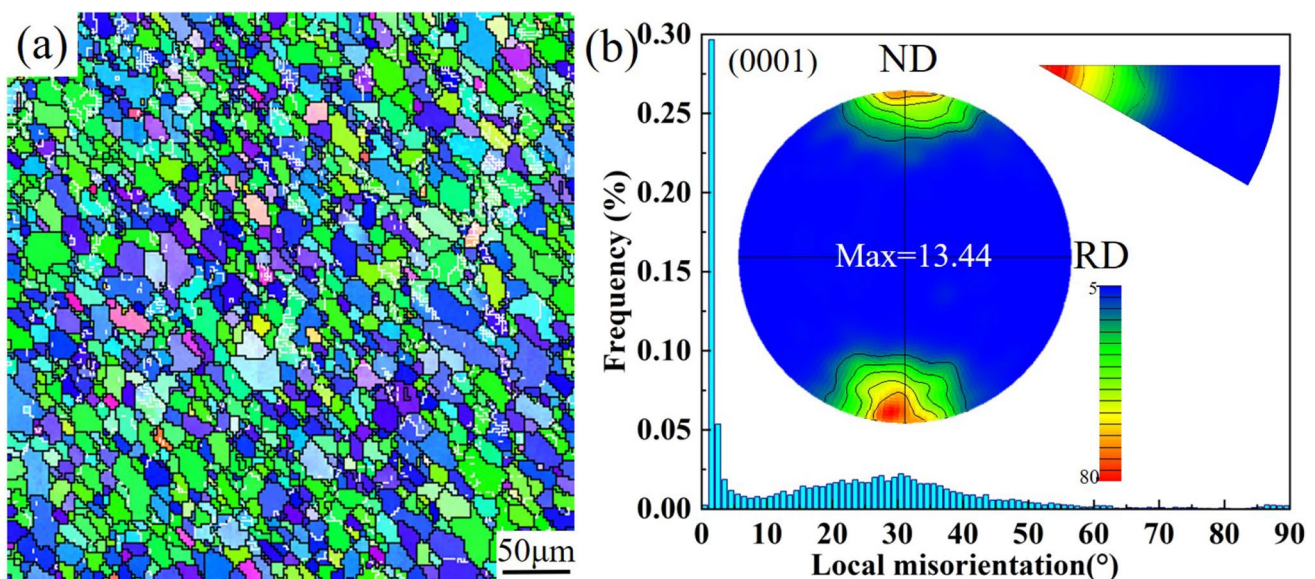


Fig. 7 Magnesium plate tissue **a** Microstructure; **b** (0001) areal polar diagram and grain boundary orientation

dislocations accounted for only 11.3%, and the rest were high-angle grain boundaries (HAGBs, $> 15^\circ$). However, a convex peak appears at $80^\circ\sim 90^\circ$, indicating that there are a certain number of tensile twins in the microstructure.

4.3 Schmid Factor

The Schmid factor is closely related to critical shear stress (CRS), which can fully reflect the difficulty of starting the slip system in the process of metal deformation. The distribution of Schmid factor and corresponding Schmid

Factor (SF) in different directions of the rolled magnesium plate is shown in Fig. 8. Figure 8a–c) shows the IPF diagram of Schmid factor in different directions. From the figure, it could be observed that there were great differences in the color of grains in different directions. The RD slip mode is mainly substrate slip, while the TD is dominated by conical slip, while the normal direction is mainly cylindrical slip. At room temperature, Mg matrix plastic deformation only has base slip, and non-base slip is difficult to initiate. Under condition of thermal deformation, Mg matrix can have the phenomenon of

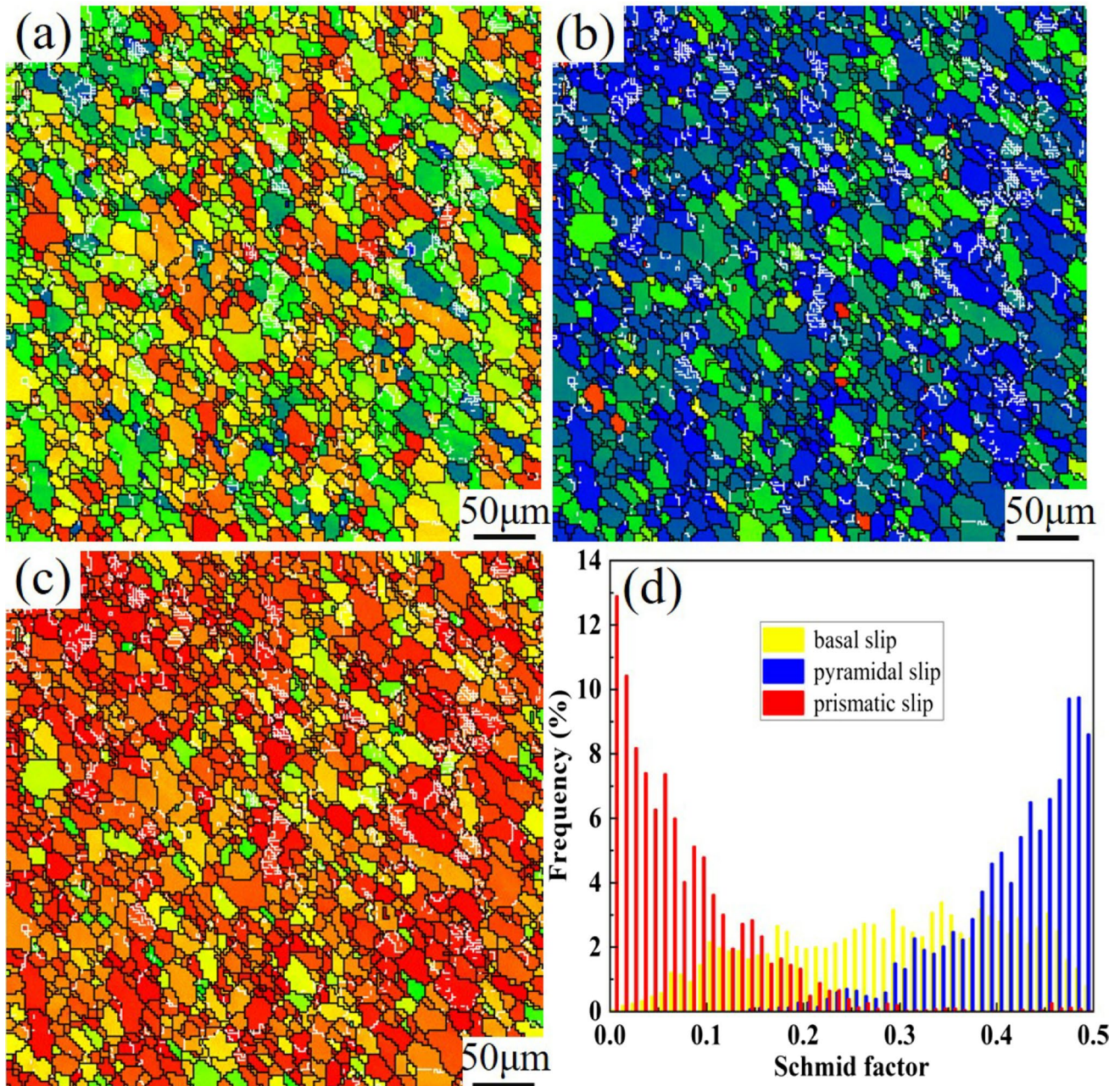


Fig. 8 Schmid factor a RD; b TD; c ND; d Poor orientation

coordinated deformation of base slip and non-base slip at the same time. Figure 8d shows that under thermal deformation, the magnesium alloy is dominated by cylindrical slip, with a frequency as high as 13.1%, while basal slip is only a minor factor. Under condition of large reduction, high stress concentration will occur at the grain boundary during rolling [24], and the stress concentration results from the accumulation of dislocations at the grain boundary and the large plastic deformation stress between adjacent grains. Critical shear stress (CRSS), as one of the components of deformation stress, is one of the key factors for the initiation of base surface slip and non-base surface slip. Shift is easy to operate. The opening of non-basal slip is a major incentive for the improvement of the plastic deformation of magnesium alloys. It is well known that the basal slip of magnesium alloys has only three slip systems, while plastic deformation requires at least five. The slip systems act simultaneously, so the actuation of the non-basal plane slip can promote the plastic deformation of the magnesium alloy, and to a certain extent, it can weaken the strength of the mixed texture.

4.4 Recrystallization Behavior

From 4.1, it can be seen that there are a large number of sub-grain boundaries that continue to rotate, leading to the gradual formation of continuous dynamic recrystallization (CDRX) at high angle grain boundaries and the nucleation and growth of discontinuous dynamic recrystallization (DDRX) at large angle grain boundaries through grain boundary migration. In order to further explore the change and evolution of recrystallization of magnesium alloy sheets, the as-rolled microstructure is analyzed.

It is discovered by Fig. 9a, b) that the liner rolled Mg plate is composed of recrystallization, sub-grain, and a large number of deformed grains, and the recrystallization distribution is uniform and did not form the “necklace” shape in the traditional liner rolling structure and coarse grains. This was because during the rolling process, the dislocations accumulated in the coarse grains provided energy for recrystallization nucleation and promoted the formation of recrystallization. However, due to the high rolling temperature, most of the recrystallized grains grew up. Figure 9d shows the proportions of recrystallized, sub-grains, and deformed grains. Among them, recrystallized grains accounted for 31.77%, sub-grains accounted

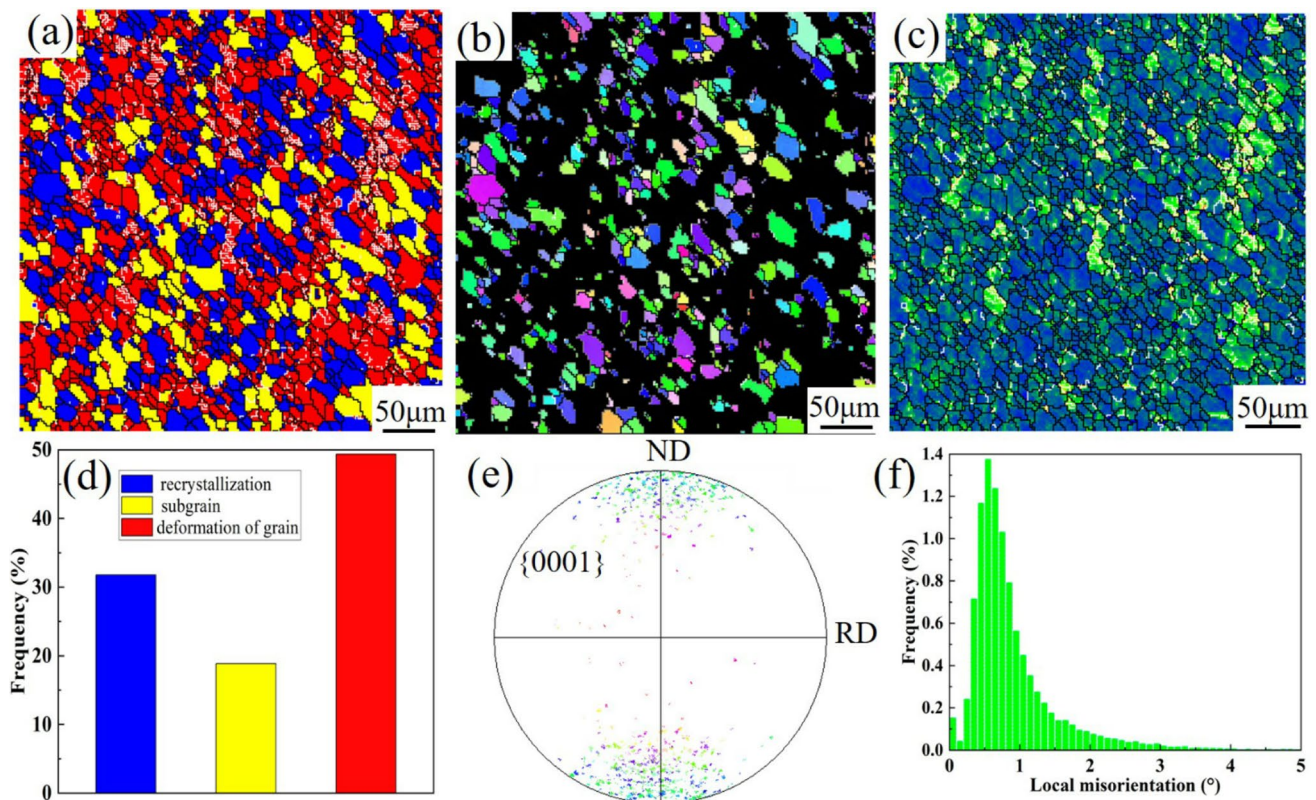


Fig. 9 Recrystallization behavior **a** Recrystallized IPF; **b** Recrystallized grains; **c** KAM; **d** Different grain proportions; **e** Pole figure; **f** KAM distribution

for 18.86%, and deformed grains accounted for 49.36%. The pole figure distribution of the recrystallized grains is shown in Fig. 9e. It can be seen that the distribution was mainly concentrated in the RD of the two poles of the ND. Due to the large local storage in the twins, it would appear in the process of induced dynamic recrystallization. The phenomenon of uneven stress distribution eventually leads to the deflection of the recrystallized grain orientation to a certain extent. As shown in Fig. 9c, kernel average misorientation (KAM) reflects the degree of homogenization of the plastic deformation of the material [25]. The blue part, with lower stored energy in the grain, dominates, and there was almost no dark part with higher energy. Combined with Fig. 9a, there was still some residual strain energy in the deformed grain. From Fig. 9f, it could be seen that a large number of dense dislocations accumulate at LAGBs, which was due to the fact that the recrystallized grains could continue to undergo GBs deformation, so that dislocations aggregate at grain boundaries, while there were fewer dislocations in HAGBs. Combined with the above analysis, it can be seen that the recrystallization nucleation and growth process of the Mg plate structure are relatively sufficient and the structure is uniform the

bonding strength and comprehensive mechanical properties of the composite board.

4.5 Twin and Deformed Grains

During the rolling process of the composite plate, there are a large number of deformed grains and small amount of tensile twins in the ND of the magnesium sheet. In order to explore its effect on the plastic deformation of magnesium sheets during rolling, two kinds of grains were analyzed separately. Figure 10 shows two different grain structures. From Fig. 10a, it can be found that the grain structure consists of various compositions. Combined with Fig. 10c KAM, it can be seen that the residual strain energy inside the grain was high, and there were a large number of sub-crystals. The orientation difference between the two points and the point to the origin is shown in Fig. 10b. It could be found from the curve that the grain orientation was constantly changing and the deflection angle reaches a peak at 7.8 m from the origin, but the orientation near the grain boundary was almost the same. In the point-to-point curve, there was mainly a large amount of deflection between adjacent parts, which was due to the climbing and entanglement of dislocations,

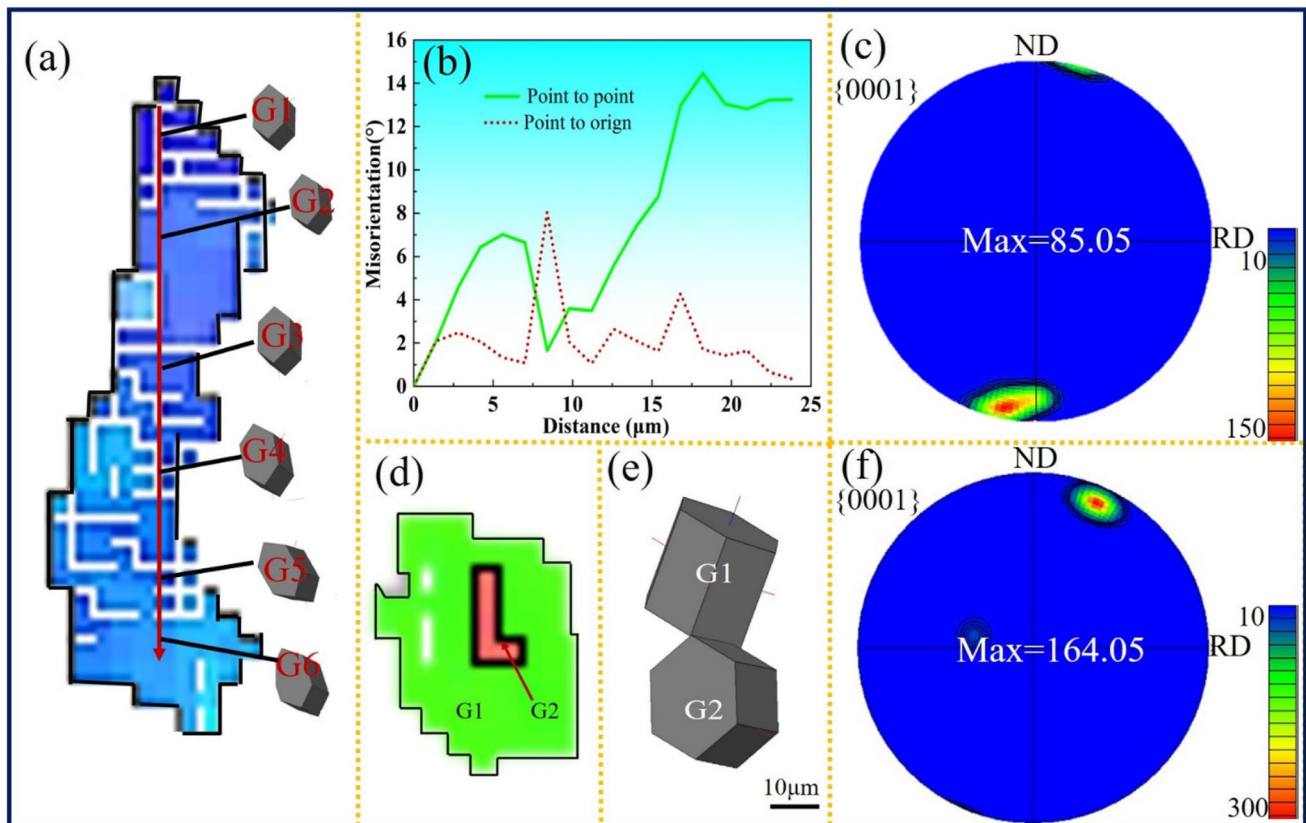


Fig. 10 Twins and deformed grains **a** Deformed grains; **b** Poor orientation; **c** Deformed grain pole diagram; **d** Twinning; **e** Grain orientation; **f** Twin pole diagram

which produced deformation energy inside the grain and twists [26]. The grains and grain orientations of twins and their precursors were shown in Fig. 10d, e). Combined with the IPF diagram of the magnesium plate, it could be found that there was a large amount of residual strain energy in the parent body, and the grain orientation of the twins had a large deviation angle compared with the parent body, which may be because the twins fail to induce recrystallization during the rolling process. The strain energy was retained in the matrix and the grains are twisted. The projected positions of deformed grains were mainly distributed at both ends of the ND direction, that is, the grain orientation RD, as shown in Fig. 10c, f), while the extremely dense region of twins was only near the ND end point. The pole density value for deformed grains is 85.05 and for twins is 164.05. The textural strength of twins is much higher than that of deformed grains. The strong texture of twins can improve the strength of the composite plate, that is, geometric strengthening, but reduce its ductility. From IPF and Fig. 10d), it can be found that twins only exist in trace amounts, mainly dominated by weakly textured deformed grains and recrystallization. Ding's research on the texture weakening of magnesium matrix by adding Ca element by hot extrusion confirmed that the comprehensive properties of the material were significantly improved after texture weakening [27]. This showed that the texture weakening anisotropy of the Mg sheet in the Al/Mg/Al composite sheet rolled by the liner was reduced, and the performance was significantly improved.

5 Conclusion

1. The research shows that the microstructure and morphology of the Mg side in the ND direction of the Al/Mg/Al composite plate rolled with a single pass and large reduction amount change greatly when the temperature k value changes. From the dominance of shear bands and twins at $k1$ to the homogenization of the structure at $k4$, and the grain growth at $k5$. At $k4$, the recrystallization ratio is as high as 31.77%, the deformed grains account for 49.36%, and the sub-crystals account for only 18.86%. Combined with KAM analysis, it is found that a large amount of residual strain energy does not appear in the deformed grains, and the degree of recrystallization is much higher than that of the traditional rolling process.
2. There are only a few twins in the Mg sheet, and the ND direction shows the phenomenon of texture weakening, and its anisotropy is significantly reduced. And under the forming conditions of $k4$, the non-base surface slip is easy to start and dominates, so that the composite plate has good plasticity and bending resistance in subsequent applications, and its maximum bending strength is as high as 504 MPa.
3. The interface of the composite plate is tightly bonded without obvious macroscopic defects. During the tearing process, the elastic deformation stage of Al is significantly longer than the tearing expansion stage and the load reaches 0.45kN. The interface bonding is uniform and the strength is high. The brittle-hard phase is produced at the interface joint, which increases the hardness of the Al side at the joint, but the hardness of the Mg side does not change significantly due to the uniform structure.

Acknowledgements This paper was supported by the Natural Science Foundation of Heilongjiang Province (No. JQ2022E004).

Declarations

Conflict of interest The authors indicate that they have no financial relationship with the organization that sponsored the research. And the authors declare that they have no conflict of interest.

References

1. Z. Yan, Z. Zhang, X. Li, J. Xu, Q. Wang, G. Zhang, J. Zheng, H. Fan, K. Xu, J. Zhu, Y. Xue, *J. Alloy. Compd.* **822**, 153698 (2020)
2. P. Wankhede, K. Suresh, *Adv. Mater. Process. Technol.* **6**, 458 (2020)
3. A. Ramesh, S. Sathian, V. Satheeshkumar, *Mater. Today Proc.* **5**, 25255 (2018)
4. K. Hassan, A.S. Kang, C. Prakash, G. Singh, *Mater. Today Proc.* **50**, 1043 (2022)
5. Y. He, H. Xu, M. Hu, B. Jiang, Z. Ji, *J. Mater. Sci. Technol.* **53**, 82 (2020)
6. Y. Wang, S. Zhang, R. Wu, N. Turakhodjaev, L. Hou, J. Zhang, S. Betsofen, *J. Mater. Sci. Technol.* **61**, 197 (2021)
7. J. Wang, L. Xu, R. Wu, J. Feng, J. Zhang, L. Hou, M. Zhang, *Acta Metall. Sin.-Engl.* **33**, 490 (2020)
8. J. Tang, L. Chen, G. Zhao, C. Zhang, J. Yu, *J. Alloy. Compd.* **784**, 727 (2019)
9. G. Chen, X. Chang, J. Zhang, Y. Jin, C. Sun, Q. Chen, Z. Zhao, *Met. Mater. Int.* **26**, 1574 (2020)
10. X. Bi, Y. Hu, R. Li, H. Zhao, T. Li, *J. Alloy. Compd.* **900**, 163417 (2022)
11. W.-W. Yang, X.-Q. Cao, L.-F. Wang, Z.-Q. Chen, W.-X. Wang, D.-Y. Wang, *Mat. Res.* **21**, e20180350 (2018)
12. Y. Yu, P. Yan, T. Chai, B. Yan, *Int. J. Mod. Phys. B* **36**, 2240056 (2022)
13. H.Y. Sun, D.H. Zhang, M. Ma, J.X. Zhang, W.C. Liu, *J. Mater. Eng. Perform.* **31**, 7624 (2022)
14. X.P. Zhang, T.H. Yang, S. Castagne, J.T. Wang, *Mater. Sci. Eng. A* **528**, 1954 (2011)
15. K. Wu, H. Chang, E. Maawad, W.M. Gan, H.G. Brokmeier, M.Y. Zheng, *Mater. Sci. Eng. A* **527**, 3073 (2010)
16. C.Z. Luo, W. Liang, X.R. Li, Y.J. Yao, *Mater. Sci. Forum* **747-748**, 346 (2013)
17. K.S. Lee, D.H. Yoon, H.K. Kim, Y.-N. Kwon, Y.-S. Lee, *Mater. Sci. Eng. A* **556**, 319 (2012)

18. X.P. Zhang, T.H. Yang, S. Castagne, J.T. Wang, *Mater. Sci. Eng. A* **528**, 1954 (2011)
19. P.D. Huo, F. Li, Y. Wang, X.M. Xiao, *Int. J. Adv. Manuf. Tech.* **118**, 55 (2022)
20. L. Chen, J. Tang, G. Zhao, C. Zhang, X. Chu, *J. Mater. Process. Tech.* **258**, 165 (2018)
21. P.D. Huo, F. Li, Y. Wang, R.Z. Wu, R.H. Gao, A.X. Zhang, *Mater. Design* **219**, 110696 (2022)
22. Z. Zhang, J. Zhang, J. Wang, Z. Li, J. Xie, S. Liu, K. Guan, R. Wu, *Int. J. Miner. Metall. Mater.* **281**, 30 (2021)
23. J. Rong, P.-Y. Wang, M. Zha, C. Wang, X.-Y. Xu, H.-Y. Wang, Q.-C. Jiang, *J. Alloy. Compd.* **738**, 246 (2018)
24. N. Wang, X. Chen, A. Li, Y. Li, H. Zhang, Y. Liu, *T. Nonferr. Metal. Soc.* **26**, 359 (2016)
25. Y. Wang, F. Li, Y. Wang, Y. Wang, X.M. Xiao, *J. Magnes. Alloy.* (2021). <https://doi.org/10.1016/j.jma.2021.05.007>
26. Y. Wang, F. Li, N. Bian, H.Q. Du, P.D. Huo, *J. Magnes. Alloy.* (2021). <https://doi.org/10.1016/j.jma.2021.08.035>
27. H. Ding, X. Shi, Y. Wang, G. Cheng, S. Kamado, *Mater. Sci. Eng. A* **645**, 196 (2015)

Publisher's Note Springer Nature remains neutral with regard to jurisdictional claims in published maps and institutional affiliations.

Springer Nature or its licensor (e.g. a society or other partner) holds exclusive rights to this article under a publishing agreement with the author(s) or other rightsholder(s); author self-archiving of the accepted manuscript version of this article is solely governed by the terms of such publishing agreement and applicable law.